PIBB 生物化学与生物物理进展
Progress in Biochemistry and Biophysics
2015, 42(3): 260~267
www.pibb.ac.cn

Structural and Functional Characterization of *Acinetobacter baumannii* Nucleoside Diphosphate Kinase*

HU Ying-Song[1,2], FENG Feng[1], LIU Ying-Fang[1]**
([1] *National Laboratory of Biomacromolecules, Institute of Biophysics, Chinese Academy of Sciences, Beijing* 100101, China;
[2] *The University of Chinese Academy of Sciences, Beijing* 100049, China)

Abstract *Acinetobacter baumannii* is a new threat in intensive care units (ICUs) for its multiresistance to antibiotics, but little is known about this bacterium. Nucleoside diphosphate kinase (NDK) is an evolutionarily conserved enzyme that catalyzes phosphoryl transformation between nucleosides. In our study, the crystal structure of wild type *Acinetobacter baumannii* NDK along with its mutant generated through truncation of the C-terminal arginine-threonine-arginine (RTR) residues, were solved. In comparison with *Myxococcus xanthus* NDK structure, we speculated that *Acinetobacter baumannii* NDK shared a similar catalytic mechanism with *Myxococcus xanthus*. Activity assay and CD spectra analysis revealed that E28A mutant might interrupt the secondary structure of the protein leading to declined enzymatic activity. Truncation of the C-terminal RTR residues would lead to the instability of the tertiary structure resulting in reduced kinase activity. Lys33 was a key residue for maintaining dimer interaction when RTR residues were truncated but was not sufficient to keep efficient enzymatic reaction. The structural data can provide a potential target to develop novel therapeutic approaches to overcome multiresistance of the bacterium against antibiotics.

Key words *Acinetobacter baumannii*, nucleoside diphosphate kinase (NDK), crystal structure
DOI: 10.16476/j.pibb.2014.0319

1 Introduction

Acinetobacter baumannii, a scarcely known pathogen for general public, has been recently gaining more and more attention from scientific community[1]. This bacterium is well known for its ability to resist to almost all antibiotics[2], leading to increase in health threat for immuno-compromised individuals, especially in intensive care units (ICUs)[3]. Efforts have been made to understand its mechanism of drug resistance but little is known about the bacterium.

Nucleoside diphosphate kinase (NDK) is a widely existing enzyme which is highly conserved from virus to mammals[4]. The enzyme catalyzes transfer of γ-phosphate from a nucleoside triphosphate (NTP) to a nucleoside diphosphate (NDP)[5-6]. According to previous solved structures, NDKs share homology in gene sequence, orientation of secondary as well as tertiary structure, but differ in orientation of quaternary structure[7-9]. The differences in quaternary structure lead to the enzyme's additional functions[10-11]. In bacteria, NDKs appear as dimer or tetramer[7-8], but in eukaryote as well as in archaea NDKs mostly occurs as hexamer[12]. Because of the nucleoside kinase activity, NDK is important in DNA and RNA biosynthesis[13]. Despite this, NDK is reported to take part in polysaccharide and protein synthesis as well as in energy metabolism[10,13]. In human, NDK is secreted out of cells and coordinate in cellular ATP signaling[14-15].

In this study, we solved the crystal structure of wild type NDK from *Acinetobacter baumannii*, according to which we found that the C-terminal arginine-threonine-arginine (RTR) residues generated several interactions on the dimer interface. For further

*This work was supported by grants from National Basic Research Program of China (2011CB910304, 2012CB910204).
**Corresponding author.
Tel: 86-10-64888288, E-mail: liuy@ibp.ac.cn
Received: October 31, 2014 Accepted: December 16, 2014

elucidation of the monomer-monomer interaction, we solved the crystal structure of the mutant that the C-terminal RTR residues were truncated. Our study combined structural and functional methods to characterize NDK from *Acinetobacter baumannii* with an aim to gain valuable insights about the bacterium leading to design of novel anti-bacterial drugs in the future.

2 Materials and methods

2.1 Cloning and mutagenesis

The NDK gene of *Acinetobacter baumannii* (strain SDF) was commercially synthesized (Genscript). Using polymerase chain reaction (PCR), the gene was amplified and cloned into a pET-28a vector (Novagen) with an N-terminal hexa-histidine tag. Mutations were introduced into the correct pET-28a-NDK plasmid by site-directed mutagenesis[16] using EasyPfu DNA polymerase (TransGen). Gene sequencing were carried out to verify the correct mutants.

2.2 Protein expression and purification

The correct clones were transformed into *Escherichia coli* BL21 (DE3). The cultures were grown in LB medium at 37℃ to an A_{600} value of 0.6. Protein expression was induced by addition of 0.1 mmol/L isopropylthiogalactopyranoside (IPTG) and incubated at 16℃ for 20 h. Cells were harvested by centrifugation and resuspended in lysis buffer containing 50 mmol/L Tris (pH 8.0), 150 mmol/L NaCl, 5 mmol/L $MgCl_2$ and 10 mmol/L imidazole.

After sonication, the lysate was centrifuged at 30 000 *g* for 30 min. The supernatant was applied to nickel beads (10 ml, GE Healthcare), washed three times with wash buffer containing 50 mmol/L Tris (pH 8.0), 150 mmol/L NaCl, 5 mmol/L $MgCl_2$ and 30 mmol/L imidazole, and eluted with elution buffer containing 50 mmol/L Tris (pH 8.0), 150 mmol/L NaCl, 5 mmol/L $MgCl_2$ and 200 mmol/L imidazole. The elution from affinity chromatography was then concentrated by spin concentrators (Amicon, Millipore) and purified by gel filtration chromatography (Superdex75, Amersham Biosciences) in size exclusion (SE) buffer containing 50 mmol/L Tris (pH 8.0), 150 mmol/L NaCl and 5 mmol/L $MgCl_2$. SDS-PAGE was used to analyze the peaks.

Target fractions of wild type and RTR truncation proteins were pooled and concentrated to ～200 g/L. After 2 weeks at 4℃, about half of the protein spontaneously degraded to a truncated form. The degraded protein was used for crystallization after addition of 1 mol/L N-Cyclohexyl-2-aminoethanesulfonic acid (CHES pH 9.0) to a final concentration of 100 mmol/L. For activity assay, 1 ml peak fraction of wild type protein or mutant protein was diluted to ～0.5 mg/L in SE buffer.

2.3 Crystallization and data collection

The hanging-drop vapor diffusion method was used for crystallization. Briefly, 1 μl protein solution was mixed with equal volumes of reservoir solution. NDK wild type crystals were obtained under the condition containing 0.1 mol/L potassium sodium tartrate tetrahydrate and 18% (*w*/*v*) polyethylene glycol 3350 while RTR truncation crystals were grown under the condition of 1 mol/L sodium malonate (pH 7.0), 0.1 mol/L HEPES (pH 7.0) and 0.5% (*v*/*v*) Jeffamine ED-2001 (pH 7.0).

NDK wild type crystal X-ray diffraction data were collected at beamline BL17U, Shanghai Synchrotron Radiation Facility (Shanghai, China), and were processed with HKL2000[17]. The crystal belongs to the I222 space group and its cell dimensions are a=61.73Å, b=76.96Å, c=82.24Å and $\alpha=\beta=\gamma=90°$ with only one molecule in an asymmetric unit. RTR truncation diffraction data were collected using MicroMax-007 HF X-ray source and Saturn 944HG CCD detector (Rigaku), then were processed with IMOSFLM[18–19]. Its space group is the same as wild type with smaller cell dimensions of a=60.33Å, b=75.40Å, c=82.12Å.

2.4 Structure determination and refinement

Initially, wild type structure was determined by molecular replacement (MR) method using *Burkholderia thailandensis* NDK (PDB code 4DUT) as starting model. After processing and improving using PHASER [20] and DM [21] respectively, PHENIX. AUTOBUILD[22–23] was used to get the primary model, which was then manually adjusted in COOT [24] and refined in PHENIX.REFINE [25] iteratively. The RTR truncation structure was determined using the same method as wild type except that the starting model was wild type. The R_{work} and R_{free} of wild type final model was 16.28% and 18.90% respectively, while for RTR truncation the values were 20.10% and 25.81%. The PDB accession code was 4W98 for wild type and 4WBF for RTR truncation. The structural figures used here were made using PyMOL(http://www.pymol.org/).

2.5 *In vitro* kinase activity assay

The *in vitro* kinase activity assay was carried out,

as described previously [26], in a 25 μl system which contained 400 μmol/L GTP as phosphoryl donor, 100 μmol/L ADP as substrate and 5 μl appropriately diluted enzyme. After a 2 min incubation at room temperature, 15 μl of reaction mixture was added to equal volume of luciferin-luciferase ATP detection buffer from ATPlite one-step kit (PerkinElmer) and a single measurement of luminescence was recorded after a 10 s delay on a luminometer (TD-20/20, Turner Designs). Background readings of relative luminescence units (RLU) were adjusted, whereby RLU from wild type NDK was standardized as 100%.

2.6 CD measurement

The 1 ml peak fraction of wild type protein or mutant proteins were diluted in PBS to 0.1～0.2 g/L. Put into a 1 mm path length cell, the far-ultraviolet CD spectra of wild type and mutant proteins were recorded on Chirascan-plus ACD (Applied Photophysics). According to voltage limitation, the wavelength range was 200～260 nm.

3 Results

3.1 Overall structure of wild type and RTR truncation NDK

The wild type *Acinetobacter baumannii* NDK structure consisted of four antiparallel β-strands embraced in seven α-helices (Table 1, Figure 1a). The whole structure presented a typical ferredoxin-like fold. Gel filtration experiment indicated that *Acinetobacter baumannii* NDK was eluted as a dimer in solution (data not shown). Using PISA [27] server to analyze dimer interaction (Figure 1b), the monomer-monomer interface area was 1189.4Å^2 containing eighteen hydrogen bonds and four salt bridges. The C-terminal residues (mainly RTR motif and Cys139) and α2 in one monomer altogether formed eleven hydrogen bonds and two salt bridges on dimer interface. In detail, Cys139 in C-terminal from one monomer could form one hydrogen bond with His41 from another monomer. Within α2, Glu28 of one monomer could form three hydrogen bonds with Ile20 and Gly21 of another monomer (Figure 1c) and vice versa. The extreme C-terminal residues (RTR) not only participated in four hydrogen bond formation, but also generated two salt bridges with another monomer (Figure 2b). Therefore, E28A and C-terminal RTR truncation mutant were constructed to evaluate structural and functional relationships of NDK.

Table 1 Summary of data collection and refinement statistics

		Wild type	RTR truncation
Data collection	Beamline	SSRF beamline BL17U	Rigaku MicroMax-007 HF
	Wavelength/Å	0.9792	1.5419
	Space group	I222	I222
Cell dimensions	(a, b, c)/Å	61.73, 76.96, 82.24	60.33, 75.40, 82.12
	(α, β, γ)/°	90.0, 90.0, 90.0	90.0, 90.0, 90.0
	Resolution (Outer shell)/Å	56.2-1.43 (1.47-1.43)	47.11-2.64 (2.90-2.64)
	R_{sym}[1)](Outer shell)	0.050 (0.562)	0.168 (0.619)
	$I/\sigma I$ (Outer shell)	51.0 (4.08)	7.3 (2.6)
	Completeness (Outer shell)/%	99.3 (100.0)	100.0 (100.0)
	Redundancy (Outer shell)	7.1 (7.1)	6.2 (6.3)
Refinement	Resolution (Outer shell)	27.05-1.43 (1.47-1.43)	47.11-2.64 (2.90-2.64)
	Total no. of reflection/free	36240/1793	5655/542
	R_{work}	0.163	0.201
	R_{free}[2)]	0.189	0.258
No. of atoms	Protein	1108	1066
	Water	169	34
	Ave. B-factors/(Å^2)	19.0	18.0
R. m. s. deviations[3)]	Bond lengths/Å	0.0057	0.0089
	Bond angle/°	1.004	1.102
Ramachandran plot	Favored/%	98.6	97.1
	Allowed/%	1.4	2.9
	Outlier/%	0.0	0.0

[1)] $R_{sym}=\Sigma(I-<I>)/\Sigma<I>$, where I was the intensity and $<I>$ was the average intensity of multiple measurements. The sum was for all measured reflections. [2)] R_{free} were calculated with about 5% and 10% of the reflections for wild type and RTR truncation respectively. [3)] R.m.s. deviations, root mean square deviation of bond length and angles were the deviations from ideal values.

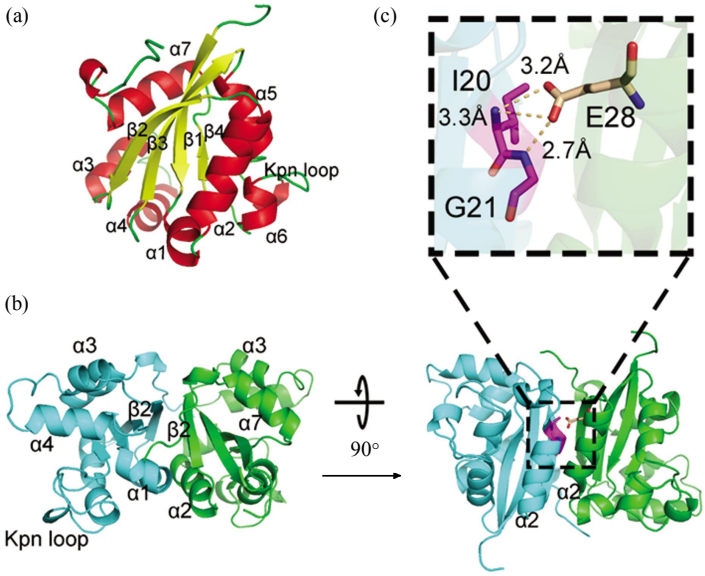

Fig. 1 Overall structure of wild type NDK

(a) Overall structure of wild type NDK, α-helices and β-strands were in different colors. (b) Dimer of wild type NDK, one monomer was green and the other was cyan. (c) Glu28 (wheat) in one monomer (green) interact with Ile20 and Gly21 (magenta) in another monomer (cyan) on the dimer interface of wild type NDK.

The RTR truncation still existed as a dimer in solution and its crystal structure determined was similar to wild type (Table 1, Figure 2a). The RMSD (root-mean-square deviation) between Cα atoms of RTR and wild type was 0.205Å. Particularly, the locations and orientations of the residues that were

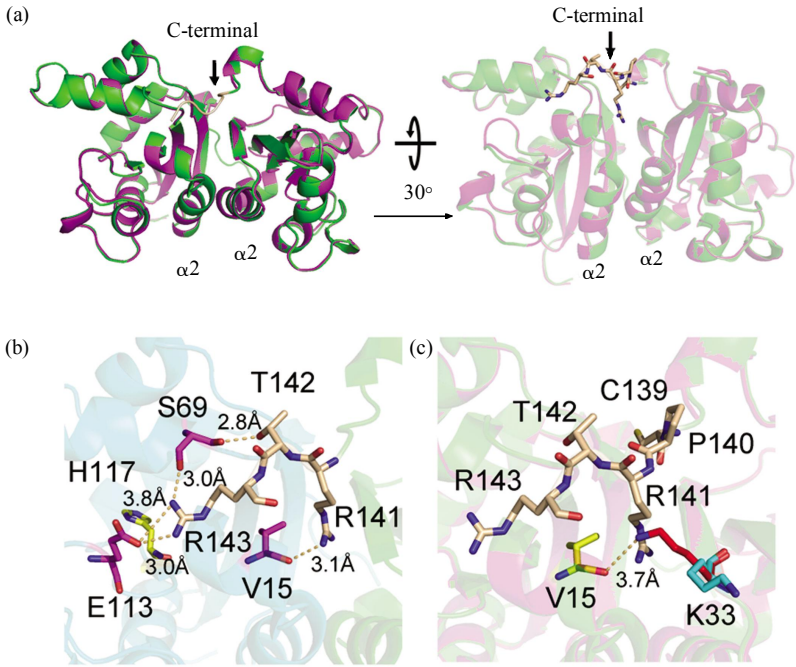

Fig. 2 Structural details of wild type NDK and its RTR truncation mutant

(a) Comparision of dimers from wild type NDK (green) and its RTR truncation mutant (magenta). The C-terminal residues CPRTR in wild type, missing in RTR truncation, were indicated as wheat. (b) RTR residues (wheat) from one monomer (green) interact with Val15, Ser69 and Glu113 (magenta) from another monomer (cyan) in wild type dimer. The active site His117 was shown in yellow. (c) Superposition of wild type (green) and RTR truncation (magenta) structure as in (a) left. The missing residues CPRTR of wild type NDK were indicated as wheat. Lys33 of wild type was painted cyan. Interaction of Lys33 (red) and Val 15 (yellow) in RTR truncation was colored light orange.

implicated to be involved in the enzymatic activity and substrate binding were almost identical in the two proteins. However, in contrast to wild type NDK, two residues next to RTR, Cys139 and Pro140 in the mutant protein, could not be found on the electron density map. In addition, Lys33 side chain in RTR truncation structure took another conformation extending to the space otherwise occupied by RTR residues in wild type structure (Figure 2c).

3.2 Structural comparison between NDK substrate binding regions of *Acinetobacter baumannii* and *Myxococcus xanthus*

Acinetobacter baumannii and *Myxococcus xanthus* NDK shared 65.03% sequence similarity and were not hexamer. Superposition of *Acinetobacter baumannii* and *Myxococcus xanthus* NDK resulted in a RMSD of 0.532Å. All the residues reported to participate in protein-ADP (adenosine diphosphate) interaction in *Myxococcus xanthus* NDK (Mx-NDK)[7] were conserved in *Acinetobacter baumannii* NDK (Ab-NDK) (Figure 3a). Among all ADP-interacting residues, His54, Thr93 and Ile111 in Ab-NDK displayed shifts of 1.5Å, 1.2Å and 1.4Å respectively in Cα atom compared to ADP-free Mx-NDK. These residues sit on the loops undergoing conformational change during enzymatic reaction, so the ~1Å shift of the residues should not have much influence on the binding of substrates. The other key residues in Ab-NDK all took conformations similar to ADP-free Mx-NDK. In addition, the electrostatic potential on the surface of Ab-NDK displayed a positively-charged pocket to hold ADP, which was consistent with Mx-NDK (Figure 3b). Therefore, the structure of Ab-NDK allowed accommodation of ADP in the similar way as Mx-NDK, demonstrating that the catalytic mechanism of Ab-NDK might bear strong resemblance with that of Mx-NDK.

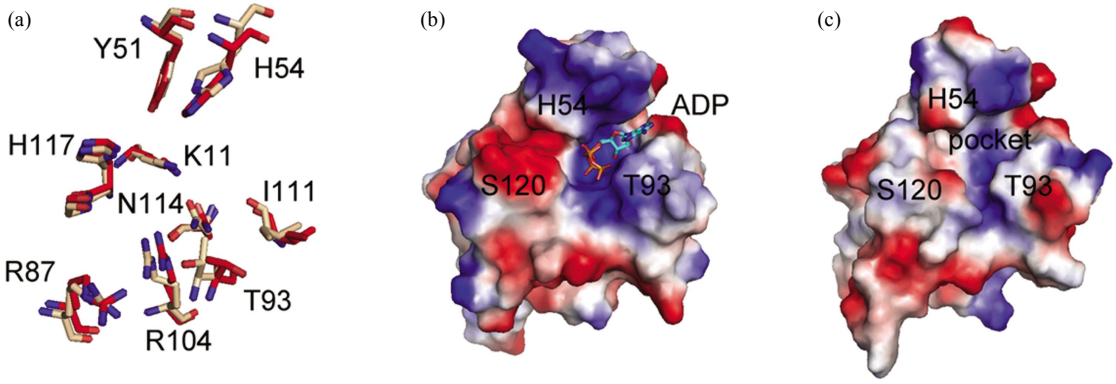

Fig. 3 Comparison of *Acinetobacter baumannii*(Ab-NDK) and *Myxococcus xanthus* NDK (Mx-NDK)

(a) Superposition of key residues participating in ADP binding between Ab-NDK (wheat) and Mx-NDK (red) (PDB code 2NCK). (b) Surface electrostatic potential of Mx-NDK (left) (PDB code 1NLK) and Ab-NDK (right). ADP in Mx-NDK was shown in sticks.

3.3 Enzymatic activities of wild type NDK and mutants

The *in vitro* enzymatic activity assay was carried out under conditions that substrates were saturated. As reported earlier, His115 (in *Acinetobacter baumannii* NDK His117) was predicted to be catalytic active site of the *Staphylococcus aureus* NDK. Mutation of this residue to a glutamine (H115Q) impaired the enzymatic activity of the protein[28]. Therefore, we used H117Q as negative control. Considering wild type NDK activity as 100%, H117Q was only 4.4% while RTR truncation was 5.3% . The kinase activity of E28A was 18.6% which was larger than RTR truncation but still reduced compared to wild type (Figure 4a).

3.4 CD analysis of secondary structure

The CD spectra of *Acinetobacter baumannii* NDK wild type and mutants were recorded to compare their secondary structures (Figure 4b). E28A showed different spectral pattern to wild type which indicated that E28A mutation changed the secondary structure of NDK. By contrast, RTR truncation showed little change in secondary structure. Compared to wild type, E28A α-helix changed from 54.62% to 48.57%. While

β-strand in wild type was 9.59%, E28A kept the level to 10.11%. Coiled coil of E28A rose to about 25% compared to 21.46% in wild type. RTR truncation kept the proportion of secondary element consistent with wild type NDK.

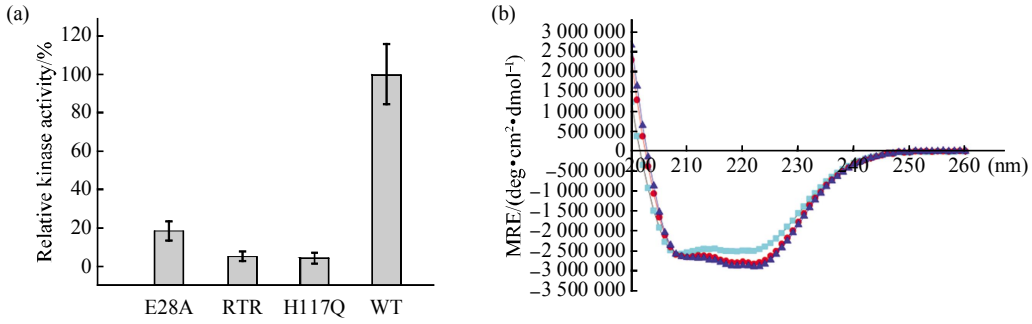

Fig. 4 *In vitro* kinase activity assay and the far-ultraviolet CD spectra of NDK mutants

(a) *In vitro* kinase activity assay. The reactions were carried out under conditions containing 400 μmol/L GTP, 100 μmol/L ADP and 5 μl appropriately diluted enzyme for 2 min at room temperature. Relative luminescence units (RLU) were recorded and compared for activity assay. Results were shown as means ± S.D. of three independent experiments. (b) The CD spectra of NDK mutants. Curves were superimposed at 208 nm. The MRE (mean residue ellipticity) was painted against the wavelength. ■—■: E28A; ●—●: RTR; ▲—▲: WT.

4 Discussions

Glu28 was relevant in secondary structure formation. According to results from CD spectra, E28A changed the secondary structure of NDK. Unlike E40K in *Pyrobaculum aerophilum* which promoted dimer interaction[12, 29], mutation E28A resulted in loss of α-helix in the whole structure but left β-strands undisturbed. At the same time, E28A showed reduced enzymatic activity which was a natural result of secondary structural change inducing the enzyme conformationally unstable.

Truncation of the C-terminal RTR residues may lead to instability of tertiary structure resulting in reduced kinase activity. Unlike E28A, the RTR truncation showed low levels of kinase activity, but had little change in the secondary structure, as observed in CD spectra. We speculated that this phenomenon might be caused by influence on NDK C-terminal mediated interaction. Therefore, we attempted to solve the crystal structure of RTR truncation. We observed that the detailed structure of RTR truncation was almost identical to the wild type except for five missing C-terminal residues on the density map. However, ten out of eighteen hydrogen bonds and all four salt bridges presenting between monomers were lost due to deletion of RTR residues. Among these, the interaction between Arg143 and Glu113 was closely adjacent to the active site His117 (Figure 2b). This interaction might influence conformational change during enzymatic reaction. It was likely that the C-terminal tail of one monomer could function like a thumbtack to consolidate tertiary structure of another monomer and reinforce monomer-monomer interaction. This C-terminal thumbtack could keep the whole structure of NDK compact and efficient during the dynamic process of catalytic reaction. As such, deletion of C-terminal RTR residues should make NDK tertiary structure unstable during phosphor-transformation reaction and result in decreased catalytic activity.

In RTR truncation structure, we also observed that Lys33 side chain extruded towards an opposite direction compared to wild type. When RTR residues were truncated, the space occupied by them was released and Lys33 side chain swayed in its position, forming hydrogen bond with Val15 from another monomer. This extra interaction might help to maintain the tertiary and dimer structure of RTR but was still weak for maintaining increased enzymatic reaction.

NDK catalyzes transfer of γ-phosphate from an NTP to an NDP. In our study, we could not get the crystal structure of Ab-NDK bound to its substrate, but

we could speculate catalytic details from other species. In *Myxococcus xanthus*, the adenine ring of ADP has only stacking interaction with Phe59 while the ribose and pyrophosphate mediate most interactions with the protein. The 3'-OH of the ribose ring form hydrogen bonds with Lys11 and Asn114. The α-phosphate may interact with His54. Next to the α-phosphate, the β-phosphate not only forms salt bridge with Lys11, Arg87 and Arg104, but also form hydrogen bonds with His117 and Tyr51[7]. All the residues interacting with ADP are conserved in *Acinetobacter baumannii* indicating a similar way of substrate binding. In *Staphylococcus aureus*, native NDK, substrate-NDK complex and NDK-ADP-vanadate structure give us an overview of the dynamic reaction[28], wherein ND1 of His115 (His117 in *Acinetobacter baumannii*) acts as nucleophile to transfer the γ-phosphate. In the NDK-ADP-vanadate structure of *Staphylococcus aureus* (which mimics the transition state of phosphor-transformation reaction), the movement of substrate γ-phosphate towards active site involve residues Tyr49, Thr91 and Arg102, while Lys9 and Val109 interact with the ribose of substrate. Accordingly, residues Tyr51, Thr93, Arg104, Lys11 and Ile111 in *Acinetobacter baumannii* are all in similar location and orientation, in order to perform the same reaction in a similar way.

In summary, by comparing the NDK structure from *Acinetobacter baumannii* with that from *Myxococcus xanthus* and *Staphylococcus aureus*, we could speculate that the catalytic mechanism of Ab-NDK should be similar to Mx-NDK. Besides, our structural and functional data of Ab-NDK revealed the significant role of Glu28 and RTR residues on the kinase activity of NDK. These results expand our understanding of *Acinetobacter baumannii* and NDK, which can provide a potencial target to develop novel therapeutic approaches to overcome multiresistance of the bacterium against antibiotics.

Acknowledgements We thank following people from Institute of Biophysics, CAS, for their kindly help. We thank Dr. GAO Guang-Xia for providing luminometer to do enzymatic assay. We thank Dr. LIANG Huan-Huan for the help in data collection and processing. We thank Dr. LI Jian and LI Jun for the help in structure determination. We thank Dr. KANG Yan-Yong and Dr. Bhargavi M. BORUAH for the valuable suggestions on this manuscript.

References

[1] Howard A, O'donoghue M, Feeney A, *et al*. *Acinetobacter baumannii*: an emerging opportunistic pathogen. Virulence, 2012, **3**(3): 243-250

[2] Montefour K, Frieden J, Hurst S, *et al*. *Acinetobacter baumannii*: an emerging multidrug-resistant pathogen in critical care. Crit Care Nurse, 2008, **28**(1): 15-25; quiz 26

[3] Bonnin R A, Nordmann P, Poirel L. Screening and deciphering antibiotic resistance in *Acinetobacter baumannii*: a state of the art. Expert Rev Anti Infect Ther, 2013, **11**(6): 571-583

[4] Spooner R, Yilmaz O. Nucleoside-diphosphate-kinase: a pleiotropic effector in microbial colonization under interdisciplinary characterization. Microbes Infect, 2012, **14**(3): 228-237

[5] Mourad N, Parks R E, Jr. Erythrocytic nucleoside diphosphokinase. II. Isolation and kinetics. J Biol Chem, 1966, **241**(2): 271-278

[6] Agarwal R P, Parks R E, Jr. Erythrocytic nucleoside diphosphokinase. V. Some properties and behavior of the pI 7.3 isozyme. J Biol Chem, 1971, **246**(7): 2258-2264

[7] Williams R L, Oren D A, Munoz-Dorado J, *et al*. Crystal structure of *Myxococcus xanthus* nucleoside diphosphate kinase and its interaction with a nucleotide substrate at 2.0 A resolution. J Mol Biol, 1993, **234**(4): 1230-1247

[8] Moynie L, Giraud M F, Georgescauld F, *et al*. The structure of the *Escherichia coli* nucleoside diphosphate kinase reveals a new quaternary architecture for this enzyme family. Proteins-Structure Function and Bioinformatics, 2007, **67**(3): 755-765

[9] Wang H, Bao R, Jiang C H, *et al*. Structure of Ynk1 from the yeast *Saccharomyces cerevisiae*. Acta Crystallogr F, 2008, **64** (7): 572-576

[10] Gong L, Wu Z, Guo L, *et al*. Metastasis suppressor Nm23-H1 inhibits STAT3 signaling *via* a negative feedback mechanism. Biochem Biophys Res Commun, 2013, **434**(3): 541-546

[11] Dexheimer T S, Carey S S, Zuohe S, *et al*. NM23-H2 may play an indirect role in transcriptional activation of c-myc gene expression but does not cleave the nuclease hypersensitive element Ⅲ(1). Mol Cancer Ther, 2009, **8**(5): 1363-1377

[12] Pedelacq J D, Waldo G S, Cabantous S, *et al*. Structural and functional features of an NDP kinase from the hyperthermophile crenarchaeon Pyrobaculum aerophilum. Protein Sci, 2005, **14**(10): 2562-2573

[13] Chakrabarty a M. Nucleoside diphosphate kinase: role in bacterial growth, virulence, cell signalling and polysaccharide synthesis. Mol Microbiol, 1998, **28**(5): 875-882

[14] Bours M J L, Swennen E L R, Di Virgilio F, *et al*. Adenosine 5 '-triphosphate and adenosine as endogenous signaling molecules in immunity and inflammation. Pharmacol Therapeut, 2006, **112**(2): 358-404

[15] Yilmaz O, Yao L, Maeda K, *et al*. ATP scavenging by the intracellular pathogen Porphyromonas gingivalis inhibits P2X7-mediated host-cell apoptosis. Cell Microbiol, 2008, **10**(4): 863-875

[16] Hemsley A, Arnheim N, Toney M D, *et al*. A simple method for site-directed mutagenesis using the polymerase chain-reaction. Nucleic Acids Res, 1989, **17**(16): 6545−6551

[17] Otwinowski Z, Minor W. Processing of X-ray diffraction data collected in oscillation mode. Method Enzymol, 1997, **276**: 307−326

[18] Bailey S. The Ccp4 suite - programs for protein crystallography. Acta Crystallogr D, 1994, **50**(5): 760−763

[19] Powell H R, Johnson O, Leslie a G W. Autoindexing diffraction images with iMosflm. Acta Crystallogr D, 2013, **69**(7): 1195−1203

[20] Mccoy a J, Grosse-Kunstleve R W, Adams P D, *et al*. Phaser crystallographic software. J Appl Crystallogr, 2007, **40**(4): 658−674

[21] Cowtan` K D. 'dm': An Automated Procedure for Phase Improvement by Density Modification`, Joint CCP4 and ESF-EACBM newsletter on protein crystallography, 1994, **31**: 34−38

[22] Adams P D, Afonine P V, Bunkoczi G, *et al*. PHENIX: a comprehensive Python-based system for macromolecular structure solution. Acta Crystallogr D Biol Crystallogr, 2010, **66** (Pt 2): 213−221

[23] Cowtan K. The Buccaneer software for automated model building. 1. Tracing protein chains. Acta Crystallogr D Biol Crystallogr, 2006, 62(Pt 9): 1002−1011.

[24] Emsley P, Cowtan K. Coot: model-building tools for molecular graphics. Acta Crystallogr D Biol Crystallogr, 2004, **60**(Pt 12 Pt 1): 2126−2132

[25] Davis I W, Murray L W, Richardson J S, *et al*. MolProbity: structure validation and all-atom contact analysis for nucleic acids and their complexes. Nucleic Acids Res, 2004, **32** (web server issue): W615−W619

[26] Buxton I L. Inhibition of Nm23H2 gene product (NDPK-B) by angiostatin, polyphenols and nucleoside analogs. Proc West Pharmacol Soc, 2008, **51**: 30−34

[27] Krissinel E, Henrick K. Detection of protein assemblies in crystals. Lect Notes Comput Sc, 2005, **3695**: 163−174

[28] Srivastava S K, Rajasree K, Gopal B. Conformational basis for substrate recognition and regulation of catalytic activity in *Staphylococcus aureus* nucleoside di-phosphate kinase. Biochim Biophys Acta, 2011, **1814**(10): 1349−1357

[29] Pedelacq J D, Piltch E, Liong E C, *et al*. Engineering soluble proteins for structural genomics. Nat Biotechnol, 2002, **20** (9): 927−932

鲍曼不动杆菌核苷二磷酸激酶的结构和功能研究 *

胡颖嵩[1, 2)] 冯 峰[1)] 刘迎芳[1)**]

([1)] 中国科学院生物物理研究所，北京 100101；[2)] 中国科学院大学，北京 100049)

摘要 近年来，鲍曼不动杆菌(*Acinetobacter baumannii*)在医院里越来越受到人们的关注，尤其是在重症监护病房(ICUs)．它以强大的多重耐药性(multiresistance)而闻名．核苷二磷酸激酶(nucleoside diphosphate kinase，NDK)是一种进化上非常保守的酶，它能催化核苷之间磷酸基团的转移．我们解析了鲍曼不动杆菌 NDK 野生型和 C 端氨基酸残基 Arg141-Thr142-Arg143 (RTR)截短突变体的结构．通过和黄色黏菌(*Myxococcus xanthus*)NDK 的三维结构进行比较，推断鲍曼不动杆菌 NDK 的催化机制和黄色黏菌类似．通过激酶活性实验和圆二色谱实验，发现鲍曼不动杆菌 NDK E28A 突变体二级结构发生了改变，从而导致蛋白催化活性降低，说明 Glu28 是鲍曼不动杆菌 NDK 结构中非常关键的氨基酸残基．鲍曼不动杆菌 NDK C 端 RTR 截短突变体显示出催化活性极大的降低，这可能与 C 端 RTR 残基介导的二体间相互作用有关．虽然 RTR 截短突变体中的 Lys33 伸向了和野生型中不同的方向，和 Val15 产生相互作用弥补了一部分因为 RTR 截短丢失的相互作用，维持了 RTR 截短突变体和野生型类似的结构．但是，Lys33 产生的相互作用依然太弱，不足以维持蛋白在催化的动态过程中整体结构的高效转换．我们解析的鲍曼不动杆菌 NDK 晶体高分辨率结构将有助于科学家设计针对鲍曼不动杆菌的药物．

关键词 鲍曼不动杆菌，核苷二磷酸激酶(NDK)，晶体结构

学科分类号 Q5，Q6 **DOI**: 10.16476/j.pibb.2014.0319

* 国家重点基础研究发展计划(973)资助项目(2011CB910304，2012CB910204).

** 通讯联系人.

Tel: 010-64888288, E-mail: liuy@ibp.ac.cn

收稿日期：2014-10-31，接受日期：2014-12-16